

# Kohn-Sham Exchange Potential for a Metallic Surface

C. M. Horowitz, C. R. Proetto and S. Rigamonti

*Centro Atómico Bariloche and Instituto Balseiro, 8400 S. C. de Bariloche, Río Negro, Argentina*

The behavior of the surface barrier that forms at the metal-vacuum interface is important for several fields of surface science. Within the Density Functional Theory framework, this surface barrier has two non-trivial components: exchange and correlation. Exact results are provided for the exchange component, for a jellium metal-vacuum interface, in a slab geometry. The Kohn-Sham exact-exchange potential  $V_x(z)$  has been generated by using the Optimized Effective Potential method, through an accurate numerical solution, imposing the correct boundary condition. It has been proved analytically, and confirmed numerically, that  $V_x(z \rightarrow \infty) \rightarrow -e^2/z$ ; this conclusion is not affected by the inclusion of correlation effects. Also, the exact-exchange potential develops a shoulder-like structure close to the interface, on the vacuum side. The issue of the classical image potential is discussed.

Density Functional Theory (DFT) is a successful theory to calculate the electronic structure of atoms, molecules, clusters, and solids. Its goal is the quantitative understanding of materials properties starting from the fundamental laws of quantum mechanics. It is then a major drawback of DFT[1], that when applied in its highly successful Local Density Approximation (LDA) to the metal-vacuum interface system, it yields an exponential vanishing exchange-correlation (xc) potential which fails to reproduce the image-like asymptotic behavior of the surface barrier[2]. This problem of LDA is common to all local or semi-local extensions of it (GGA, meta-GGA,...). More importantly, the issue of the long-range behavior of the surface barrier is not even settled from the conceptual point of view, being still unclear the relative importance of exchange and correlation in determining this image-like decay[3]. The aim of this work is to provide a rigorous state-of-the-art calculation of the exchange component of the Kohn-Sham surface barrier for the simplest model of a jellium metal-vacuum interface. We have found that  $V_x(z)$  behaves as  $-e^2/z$  for large  $z$  in the vacuum region, and that it presents a shoulder close to the interface, although mainly located in the vacuum side. These findings are of great importance for the interpretation of a variety of surface sensitive experiments[3].

Our calculations are restricted to the slab-jellium model of a metallic surface, where the discrete character of the positive ions inside the metal is replaced by a uniform distribution of positive charge (the jellium). The positive jellium density is given by  $n_+(z) = \bar{n} \theta(d/2 - |z + d/2|)$ , which describes a slab of width  $d$ , with jellium edges at  $z = -d, 0$ . The model is invariant under translations in the  $x, y$  plane (area  $A$ ), so the wave-functions of the auxiliary Kohn-Sham system can be factorized as  $\varphi_{i\mathbf{k}}(\mathbf{r}) = e^{i\mathbf{k} \cdot \boldsymbol{\rho}} \xi_i(z)/\sqrt{A}$ , where  $\boldsymbol{\rho}$  and  $\mathbf{k}$  are the in-plane coordinate and wave-vector, respectively.  $\xi_i(z)$  are the normalized spin-degenerate eigenfunctions for electrons in slab discrete levels  $i$  ( $= 1, 2, \dots$ ), and energy  $\varepsilon_i$ . Within the Kohn-Sham implementation of DFT,

they are the solutions of

$$\hat{h}_{\text{KS}}^i(z) \xi_i(z) \equiv \left[ \frac{-\hbar^2}{2m_0} \frac{\partial^2}{\partial z^2} + V_{\text{KS}}(z) - \varepsilon_i \right] \xi_i(z) = 0. \quad (1)$$

The KS potential is the sum of several contributions:  $V_{\text{KS}}(z) = V_{\text{H}}(z) + V_{xc}(z)$ .  $V_{\text{H}}(z)$  is the classical (electrostatic) Hartree potential.  $V_{xc}(z)$  is the non-classical xc contribution; it is given by  $V_{xc}(z) = \delta E_{xc} / \delta n(z)$ .  $E_{xc} \equiv E_{xc}[\{\varepsilon_i\} \{\xi_i\}]$  is the xc contribution to the total energy-functional, and  $n(z) = \sum_i^{\text{occ.}} (k_F^i)^2 |\xi_i(z)|^2 / 2\pi$  is the 3D density, with  $k_F^i = \sqrt{2m_0(\varepsilon_F - \varepsilon_i)} / \hbar$ .  $\varepsilon_F$  is the metal Fermi energy, given by the neutrality condition  $\varepsilon_F = \hbar^2 k_F^2 / 2m_0 + V_{\text{KS}}(-d/2)$ , with  $k_F = (3\pi^2 \bar{n})^{1/3}$ . The Optimized Effective Potential (OEP) method of DFT has been specially designed for dealing with wave-function and eigenvalue dependent  $E_{xc}$ , as is our case[4]. After some lengthy but standard manipulations of the OEP scheme, the calculation of  $V_{xc}(z) = V_{xc,1}(z) + V_{xc,2}(z)$  for real  $\xi_i(z)$ 's and  $E_{xc}$  functionals which only depends on occupied subbands can be summarized in the following set of equations[5],

$$V_{xc,1}(z) = \sum_i^{\text{occ.}} \frac{[k_F^i \xi_i(z)]^2}{2\pi n(z)} \left[ u_{xc}^i(z) + \Delta \bar{V}_{xc}^i \right], \quad (2)$$

$$V_{xc,2}(z) = \sum_i^{\text{occ.}} (\varepsilon_F - \varepsilon_i) \frac{(k_F^i)^2 \psi_i(z) \xi_i(z) + \psi_i'(z) \xi_i'(z)}{\pi n(z)}, \quad (3)$$

where the “shifts”  $\psi_i(z)$  are given by

$$\psi_i(z) = \sum_{j \neq i} \xi_j(z) \int_{-\infty}^{\infty} \xi_j(z') \frac{\Delta V_{xc}^i(z')}{(\varepsilon_j - \varepsilon_i)} \xi_i(z') dz', \quad (4)$$

with primes denoting derivatives with respect to  $z$ . Here,  $\Delta V_{xc}^i(z) = V_{xc}(z) - u_{xc}^i(z)$ ,  $u_{xc}^i(z) = [4\pi/A(k_F^i)^2 \xi_i(z)] \delta E_{xc} / \delta \xi_i(z)$ , and mean values (for later use) are defined as  $\bar{O}^i = \int \xi_i(z) O(z) \xi_i(z) dz$ . Eqs.(1)-(3) have to be solved self-consistently. Several comments are worth here: a) Eqs.(2)-(4) are a set of integral equations for the local (multiplicative) xc potential; b) The shifts

are invariant under the replacement  $V_{xc}(z) \rightarrow V_{xc}(z) + \alpha$ , with  $\alpha$  a constant. This means that the above set of equations determines  $V_{xc}(z)$  up to an additive constant, that should be fixed by imposing some suitable boundary condition. This is a general property of all DFT calculations for fixed number of particles, as is the present case; *c)* If the shifts are forced to be identically zero, the only term that survives is  $V_{xc,1}(z)$ . This is exactly the KLI approximation[4], which brings the identification  $V_{xc,1}(z) = V_{xc}^{\text{KLI}}(z)$ . All results given until this point include both exchange and correlation. Unless stated otherwise, we will concentrate now in the  $x$ -only case, where  $E_{xc} \rightarrow E_x$ [6].

The long-range behavior of  $V_x(z)$  in the vacuum region is an important point, that could be obtained for our slab geometry directly from Eqs.(2), (3). For this, first note that by assuming that  $V_{KS}(z \rightarrow \infty) \rightarrow 0$  (which is equivalent to the assumption that  $V_x(z \rightarrow \infty) \rightarrow 0$ ), from Eq.(1) we obtain that  $\xi_i(z \rightarrow \infty) \rightarrow e^{-z\sqrt{-2m_0\varepsilon_i}/\hbar}$  for all occupied  $i$  (disregarding a factor involving powers of  $z$ ). Following the analysis of Refs.[7] and[8], one can derive also that  $\psi_{i < m}(z \rightarrow \infty) \rightarrow e^{-z\sqrt{-2m_0\varepsilon_m}/\hbar}$ , and that  $\psi_m(z \rightarrow \infty) \rightarrow e^{-z\sqrt{-2m_0\varepsilon_{m-1}}/\hbar}$ . Here,  $i = m$  is the last occupied slab discrete level. Armed with these results, the asymptotic limit of  $V_x(z)$  is immediate:  $V_{x,2}(z)$  tends exponentially to zero, while  $V_{x,1}(z \rightarrow \infty) \rightarrow u_x^m(z) + \Delta\bar{V}_x^m$ . Besides, as  $u_x^m(z \rightarrow \infty) \rightarrow 0$  (see below), we conclude that  $V_x(z \rightarrow \infty) \rightarrow V_{x,1}(z \rightarrow \infty) \rightarrow \Delta\bar{V}_x^m$ . Consistency with the starting assumption  $V_x(z \rightarrow \infty) \rightarrow 0$ , yields the important constraint  $\Delta\bar{V}_x^m = \bar{V}_x^m - \bar{u}_x^m = 0$ . This constraint fixes the undetermined constant in  $V_x(z)$  discussed above. All numerical results of this work have been obtained by using this constraint as boundary condition. We have achieved the self-consistent numerical solution of Eqs.(1)-(3) by two different methods: *i)* direct calculation of the shifts[9], through the solution of the inhomogeneous differential equation which results from application of the operator  $\hat{h}_{KS}^i(z)$  to the shifts of Eq.(4); and *ii)* direct solution of the OEP integral equation for  $V_x(z)$ , that is exactly equivalent and can be obtained from Eqs.(2)-(3)[10]. Both methods agree in their results within numerical accuracy, although the first approach using the shifts is faster in computer time than the second. Both methods face numerical instabilities beyond a critical coordinate  $z$  in the vacuum region.

We start by presenting in Fig.1 numerical results for  $V_x(z)$ , running from relatively high (Al) to low (Rb) typical metallic densities[11]. The exact-exchange potential shows large-amplitude oscillations in the metallic side close to the jellium edge[2], strongly depends on density in the bulk-like region at the slab center, and develops a “shoulder” close to the jellium edge, on the vacuum side. For an homogeneous 3D electron gas  $V_x(z)$  becomes a constant, given by  $V_x(3D) = -(18/\pi^2)^{1/3}/r_s \simeq -0.122/r_s$ . Replacing in this expression for  $V_x(3D)$  the

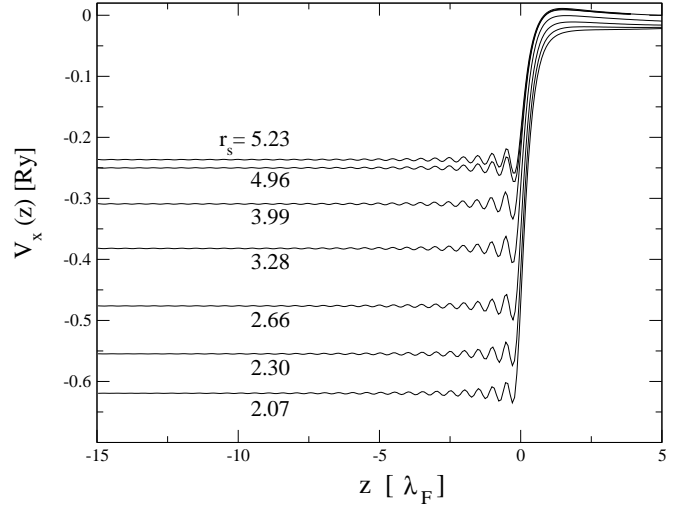


FIG. 1: Dependence of  $V_x(z)$  on jellium density, for a fixed slab width  $d = 30 \lambda_F$ . Jellium edge at  $z = 0$ , slab center at  $z = -d/2 = -15 \lambda_F$ .  $z \geq 0$  corresponds to the vacuum region. Note that as  $\lambda_F = (32\pi^2/9)^{1/3}r_s a_0$ , the thickness of each slab (in units of  $a_0$ ) increases from bottom to top.

$r_s$  values of Fig.1, we obtain  $-0.590$  (Al),  $-0.531$  (Pb),  $-0.459$  (Mg),  $-0.372$  (Li),  $-0.306$  (Na),  $-0.246$  (K), and  $-0.234$  (Rb). The results of Fig.1 for  $V_x(-d/2)$  are close to these numbers, although they are systematically more negative, due to a slab finite-size effect.

Two striking features of  $V_x(z)$  remain to be discussed: *i)* the building of a shoulder structure close to the metal-vacuum interface, and *ii)* the long-range behavior far from the jellium edge. The strength of the shoulder structure depends on density (Fig.1) and slab size (see top panel of Fig.3). We show in Fig.2 the details of the shoulder structure: it is due to the shift-dependent term in  $V_x(z)$ , that is,  $V_{x,2}(z)$ . This contribution is very small in the bulk-like region at the slab center, but exhibits oscillations when approaching the jellium edge, yielding the shoulder in the total exact-exchange potential right after the interface. It is important to note that this effect is beyond the KLI approximation, which amounts to approximate  $V_x(z)$  by  $V_{x,1}(z)$ .

The detailed asymptotic behavior of the exact-exchange potential is best discussed starting from the previous result that  $V_x(z \rightarrow \infty) \rightarrow u_x^m(z \rightarrow \infty)$ . Using the exact-exchange energy functional appropriate for a slab geometry[6], we obtain

$$u_x^m(z \rightarrow \infty) \rightarrow -e^2 k_F^m \int_{-\infty}^{\infty} \xi_m^2(y) F(k_F^m |z - y|) dy, \quad (5)$$

with  $F(x) = [x + L_1(2x) - I_1(2x)]/x^2$ , and  $I_1$  and  $L_1$  being the modified Bessel and Struve functions, respectively. Considering now that in the asymptotic limit  $z \gg y$ , an expansion of the functions  $I_1$  and  $L_1$  in

the limit of large arguments leads to  $F(z \gg y) \rightarrow (k_F^m z)^{-1} [1 + y/z - 2/(\pi k_F^m z) + \mathcal{O}(1/z^2)]$ . Inserting this in Eqs.(5), the remaining integral can be evaluated analytically, yielding the important result

$$V_x(z \rightarrow \infty) \rightarrow u_x^m(z \rightarrow \infty) \rightarrow -\frac{e^2}{z} \left(1 + \frac{\beta}{z} + \dots\right), \quad (6)$$

with  $\beta = \bar{z}^m - 2/(\pi k_F^m)$ . It is interesting to note that no explicit knowledge of  $\xi_m(z)$  is needed in passing from Eq.(5) to (6), as just normalization has been used. Let us emphasize, however, that Eq.(6) is an intrinsic slab result, as in its derivation the discrete character of the energy spectrum along the  $z$  coordinate played a crucial role. This can be made more explicit by considering that  $\bar{z}^m \sim d$  and  $k_F^m \sim 1/d$ , which allows approximate the  $\beta/z$  term in Eq.(6) as proportional to  $d/z$ . For the expansion to be valid, this term should be smaller than the leading one, implying the slab limit  $d/z < 1$ .

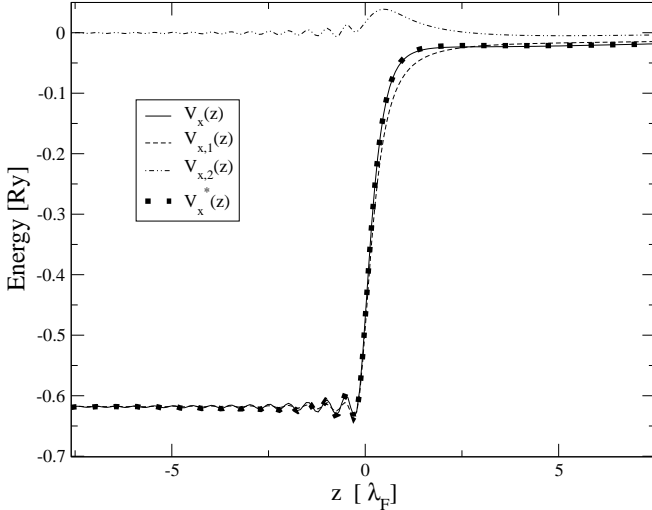


FIG. 2:  $V_x(z)$  in terms of the two components  $V_{x,1}(z)$  and  $V_{x,2}(z)$  for  $r_s = 2.07$  and  $d = 30\lambda_F$ .  $V_x^*(z)$  (full dots) corresponds to the exact-exchange potential including correlation (*a la* LDA).

The top panel of Fig.3 displays the behavior of  $V_x(z)$  in the neighborhood of the metal-vacuum interface, for  $r_s = 2.07$ , and two different slab sizes. For the narrower slab, the asymptotic regime is reached about  $7\lambda_F$ 's from the jellium edge, resulting in an excellent agreement between  $V_x(z)$  calculated numerically, and the asymptotic approximation of Eq.(5). The oscillation which appears in  $V_x(z)$ , is due to a crossover regime, where the density passes from being essentially dominated by  $\xi_{m-1}^2(z)$  to  $\xi_m^2(z)$ . For the slab with  $d = 30\lambda_F$ , the asymptotic limit moves away from the jellium edge, and a good matching is reached only between the KLI component  $V_{x,1}(z)$  and  $u_x^m(z \rightarrow \infty)$ . However, and due essentially to the fact that  $V_{x,2}(z)$  has still a sizeable value for the largest

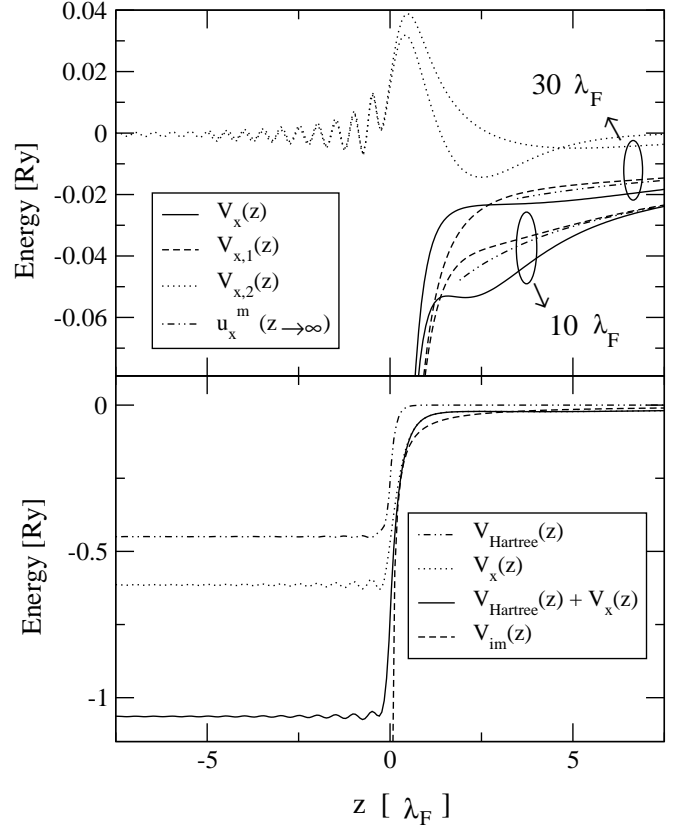


FIG. 3: Upper panel: details of  $V_x(z)$ ,  $V_{x,1}(z)$ ,  $V_{x,2}(z)$ , and  $u_x^m(z \rightarrow \infty)$  in the vacuum region, for two slab sizes. Lower panel: comparison of  $V_{KS}(z)$  with  $V_{im}(z)$ , for  $d = 30\lambda_F$ .  $r_s = 2.07$  in both panels.

$z$  coordinate within the reach of the numerical calculation, not quantitative agreement is observed yet between  $V_x(z)$  and Eq.(5). Having presented then compelling numerical evidence of the validity of Eq.(5) in representing the exact-exchange potential in the asymptotic regime, the result of Eq.(6), which follows at once from Eq.(5), is also confirmed numerically.

The long-standing puzzle of the image-potential is briefly discussed now at the light of the results presented in the lower panel of Fig.3. Already in 1936, in his pioneering study of the surface barrier at the jellium metal-vacuum interface, Bardeen considered that under the *combined* effects of exchange and correlation, electrons far enough from the jellium edge should be subject to the classical image-potential  $V_{im}(z) = -e^2/4z$ [12]. In fact, he imposed this asymptotic behavior on his approximate Hartree-Fock calculation. Many years later, the first application of DFT at the study of the same problem was performed by Lang and Kohn[2]. They used LDA, so their  $V_{xc}(z)$  vanishes exponentially as  $z \rightarrow \infty$ , as already discussed. However, they recognized that the correct  $V_{xc}(z)$  would behave like the classical image po-

tential,

$$V_{xc}(z \rightarrow \infty) \rightarrow V_{im}(z) = -e^2/4z. \quad (7)$$

Motivated by this, we have included  $V_{im}(z)$  in the lower panel of Fig.3, and compared with our exact-exchange results. As expected,  $V_{im}(z)$  decays more rapidly than our  $V_x(z)$ , and misses the shoulder which is present in the exact-exchange solution. Assuming that Eq.(7) is correct, we speculate that the apparent discrepancy with Eq.(6) is due to correlation, which is the only missing ingredient in our exact  $x$ -only calculation. This would imply that  $V_c(z \rightarrow \infty) \rightarrow 3e^2/4z$ . We emphasize, however, that this conclusion is a direct consequence of the assumption that  $V_{xc}(z \rightarrow \infty) \rightarrow V_{im}(z)$ . To the best of our knowledge, no rigorous proof inside the DFT framework exist for this equivalence[3]. As a by-product, our contribution clearly points that more work is needed on this subtle issue.

Let us place our results in the context of other related works. In Ref.[13] the asymptotic behavior of  $V_{xc}(z)$  for the case of a semi-infinite jellium surface was addressed from a many-body point of view. It was stated (without proof), that for macroscopic systems the exchange potential tends exponentially to zero, concluding that the long-range components of  $V_{xc}(z)$  can only originate from correlation effects. Similar conclusions were reached in Ref.[14] by analyzing the asymptotic limit of the Sham-Schlüter integral equation for  $V_{xc}(z)$ , except for the result that  $V_x(z \rightarrow \infty) \rightarrow -1/z^2$ , in disagreement with Ref.[13]. Being our numerical calculations restricted to finite slab geometries, we can not compare with these two ones. We would like to address, however, that our result that  $V_x(z \rightarrow \infty) \rightarrow -e^2/z$  for very thick slabs (in terms of  $\lambda_F$ ), is not in agreement with either two results. The slab calculations of Ref.[10] and Ref.[15], are much closer to ours. In Fig.10 of Ref.[10] results are shown for  $V_x(z)$ , obtained through the numerical solution of the OEP integral equation, for a slab of  $4\lambda_F$  width ( $r_s = 2.07$ ). The figure suggests that  $V_x(z) = 0$  was forced about  $1\lambda_F$  from the jellium edge, spoiling any detailed study of the asymptotic properties of  $V_x(z)$ . Using the same approach, Fig.2 of Ref.[15] present results for  $V_x(z)$  for slab thickness of about  $5\lambda_F$ , for  $r_s = 3.23$ . From the asymptotic analysis of the numerical results in their vacuum region, that only extends  $1.25\lambda_F$  from the jellium edge, the authors of Ref.[15] conclude that  $V_x(z \rightarrow \infty) \rightarrow -1/z^2$ . The results presented above suggest, however, that the correct asymptotic behavior sets in at much larger distances from the jellium edge. Also, the shoulder is not discernible in their results for  $V_x(z)$ . Our work is also not in agreement with the results of Ref.[16], where through approximate analytical techniques applied to a model slab geometry, it is claimed that  $V_x(z \rightarrow \infty) \rightarrow -1/z^2$  asymptotically.

What about correlation? Both limits  $V_x(-d/2) \rightarrow V_x(3D)$  and  $V_x(z \rightarrow \infty) \rightarrow -e^2/z$  are unchanged if correlation is included. The rigidity of the bulk-like limit is

displayed in Fig.2, where it is seen that  $V_x(z)$  does not change in the metallic region if correlation is present. This is essentially a consequence of the boundary condition  $\bar{V}_x^m = \bar{u}_x^m$ , that ensures the exact fulfillment of the exchange bulk-like limit, independently of correlation effects. The asymptotic result of Eqs.(5) and (6) are also rigorously valid even if correlation is included, as in this case each one of the basic Eqs.(2)-(4) can be splitted in an exchange and correlation components, due to the fact that  $E_{xc} = E_x + E_c$ . All the subsequent derivations leading to Eq.(6) for the exchange component of the total KS potential remains valid in consequence in the presence of correlation, that will not modify the general properties of the  $\xi_i(z)$ 's and the exchange component of the  $\psi_i(z)$ 's on which they are based, such as asymptotic behavior and normalization.

In summary, we have achieved a rigorous analytical and numerical study of the exchange component of the surface barrier at the jellium metal-vacuum interface. The Kohn-Sham exact-exchange potential develops a shoulder-like structure within  $1 - 2\lambda_F$ 's from the jellium edge, and decays as  $-e^2/z$  at much larger distances. This exchange asymptotic behavior is unperturbed by correlation. With these exact results at the exchange level, the challenge quest of DFT for a compatible energy correlation functional is now much better focalized.

CH and SR acknowledge financial support from CONICET and CNEA/CONICET, respectively. This work was partially supported by the CONICET under grant PIP 2753/00 and the ANPCyT under PICT02 03-12742.

- 
- [1] R. G. Parr and W. Yang, in *Density Functional Theory of Atoms and Molecules* (Oxford University Press, New York, 1989).
  - [2] N. D. Lang and W. Kohn, Phys. Rev. B **1**, 4555 (1970).
  - [3] J. Dobson, in *Density Functional Theory*, edited by E. K. U. Gross and R. M. Dreizler (Plenum Press, New York, 1995), p. 393; M. Nekovee and J. M. Pitarke, Comp. Phys. Comm. **137**, 123 (2001).
  - [4] J. B. Krieger, Y. Li, and G. J. Iafrate, Phys. Rev. A **45**, 101 (1992). Denoted as KLI in the text.
  - [5] S. Rigamonti, C. R. Proetto, and F. A. Reboredo, Europhys. Lett. **70**, 116 (2005).
  - [6] F. A. Reboredo and C. R. Proetto, Phys. Rev. B **67**, 115325 (2003).
  - [7] T. Kriebich *et al.*, Adv. Quantum Chem. **33**, 31 (1999).
  - [8] F. Della Sala and A. Görling, Phys. Rev. Lett. **89**, 33003 (2002).
  - [9] S. Kümmel and J. P. Perdew, Phys. Rev. Lett. **90**, 043004 (2003).
  - [10] E. Krotscheck, W. Kohn, and G.-H. Qian, Phys. Rev. B **32**, 5693 (1985).
  - [11] Numerical results are presented using the atomic Rydberg and  $\lambda_F = 2\pi/k_F$  as units of energy and length, respectively. Jellium densities are defined through the dimensionless parameter  $r_s = (3/4\pi\bar{n}a_0^3)^{1/3}$ .  $a_0$  is the Bohr

radius.

- [12] J. Bardeen, Phys. Rev. **49**, 653 (1936). It is interesting that the classical result  $V_{im}(z) = -e^2/4z$  is valid both for a semi-infinite dielectric media as for a dielectric slab (see M. Kumagai and T. Takagahara, Phys. Rev. B **40**, 12359 (1989)), as long as the dielectric constant of the slab material is much larger than the one of the surrounding material (metallic limit).
- [13] C.-O. Almbladh and U. von Barth, Phys. Rev. B **31**, 3231 (1985).
- [14] L. J. Sham, Phys. Rev. B **32**, 3876 (1985).
- [15] A. G. Eguluz *et al.*, Phys. Rev. Lett. **68**, 1359 (1992).
- [16] A. Solomatin and V. Sahni, Annals of Phys. **259**, 97 (1997).